



## State-of-charge estimation for lithium-ion batteries based on modified unscented Kalman filter using improved parameter identification

Bin Yao<sup>a</sup>, Yongxiang Cai<sup>b</sup>, Wei Liu<sup>b</sup>, Yang Wang<sup>b</sup>, Xin Chen<sup>a</sup>, Qiangqiang Liao<sup>a,\*</sup>, Zaiguo Fu<sup>a</sup>, Zhiyuan Cheng<sup>a</sup>

<sup>a</sup> Shanghai Key Laboratory of Materials Protection and Advanced Materials in Electric Power, Shanghai Engineering Research Center of Energy-Saving in Heat Exchange Systems, Shanghai University of Electric Power, Shanghai 200090, China

<sup>b</sup> Guizhou Power Grid Co., Ltd. Electric Science Research Institute, Guiyang 550002, China



### ARTICLE INFO

#### Keywords:

Lithium-ion battery  
Parameter identification  
State of charge  
Unscented Kalman filter  
First order low pass filtering algorithm

### ABSTRACT

The full and single hybrid pulse power characterization (HPPC) experiments are conducted on nickel cobalt manganese (NCM) and lithium iron phosphate (LFP) batteries to obtain the accurate relationship between state of charge (SOC) and open circuit voltage (OCV). The pseudo random number generated by the RAND function is used as the initial value of the parameter identification equation for the second-order equivalent circuit model (ECM), and the parameter identification of lithium-ion batteries is achieved through least squares fitting. The unscented Kalman filter (UKF) simulation model is modified by the first order low pass filtering (FOLPF) algorithm to improve the accuracy of SOC estimation of batteries. The results show that the goodness of fit between the real and estimated HPPC pulse voltage values at different SOC values is above 0.99 for both NCM and LFP batteries. Based on the parameter identification results, the maximum error of the HPPC voltage estimated by the second-order ECM is within 0.045 V under both full pulse and single pulse testing conditions while the maximum error of SOC estimation is within 0.025. The UKF model modified by the FOLPF algorithm provides a reference for the accurate SOC estimation of batteries.

### 1. Introduction

Lithium-ion batteries (LIBs) have emerged as the preferred choice for electric vehicles and energy storage systems due to their high energy density, low self-discharge rates, and absence of memory effect [1,2]. Key parameters in battery management systems (BMS) include state of health (SOH) [3–5], state of charge (SOC) [6–8], and remaining useful life (RUL) [9–11] of the battery. The key factor for the safe and stable operation and maintenance of the batteries system is the accurate estimation of SOC. Accurate SOC estimation is the core of BMS and a prerequisite for avoiding overcharging and discharging, thereby extending the battery life and improving its reliability and durability. The battery SOC is defined as the ratio of the remaining capacity to the nominal capacity [12]. It is one of the main parameters that reflects the operating status of batteries. However, SOC is a physical quantity that cannot be directly measured and is susceptible to factors such as charge rate, discharge rate, voltage, ambient temperature, aging, and self-discharge rate. In practice, SOC is affected by the nonlinear characteristics of

batteries and can only be estimated through measurable parameters like voltage, current, and temperature. Researchers currently face numerous challenges in SOC estimation. For instance, the complex structure of LIBs, along with the intricacies of electrochemical reaction processes and reaction stages, poses difficulties in accurately estimating SOC. Therefore, the accurate estimation of SOC remains a challenging goal for any BMS [13,14].

At present, the existing SOC estimation methods can be divided into four categories including direct estimation methods, Ampere hour integration method, model-based estimation methods, and data-driven estimation methods [15–17]. The most common SOC estimation method is the ampere hour integration method. The ampere hour integration method calculates SOC by integrating the battery current over time, making it simple and straightforward to implement. However, as an open-loop method, it cannot eliminate initial SOC errors caused by self-discharge and capacity recovery, as well as cumulative errors induced by current disturbances. Data-driven SOC estimation methods primarily contribute by learning the mapping relationships of internal

\* Corresponding author.

E-mail address: [liaoqiangqiang@shiep.edu.cn](mailto:liaoqiangqiang@shiep.edu.cn) (Q. Liao).

battery parameters from data [18]. However, the complexity of influencing factors makes it challenging to accurately determine mapping relationships that can characterize the internal behavior of the battery. Among the category of model-based estimation methods for batteries, the equivalent circuit model (ECM) is widely employed due to its simple structure, high accuracy, and ability to represent key battery characteristics, such as open-circuit voltage, ohmic resistance, and polarization effects [19]. The ECMs typically use parallel resistors and capacitors to form RC pairs, representing various physical and chemical reactions within the battery. The most commonly used ECMs include the Rint model, Thevenin model, and Dual Polarization (DP) model [20,21]. Following the establishment of a battery model, parameter identification becomes a prerequisite for accurately estimating SOC and is a critical factor influencing model accuracy.

The determination of ECM parameters for LIBs is currently achieved through two main methods: online identification and offline identification. Online identification holds potential value for SOC estimation as it can reduce the time-consuming process of offline experimental data sampling. Shi et al. [22] introduced a recursive least squares parameter identification method with a variable forgetting factor based on a sliding window mode. By utilizing the mean square value of the difference between open-circuit voltage and terminal voltage within a sliding window, the method enhances the information gleaned from new data and employs recursive least squares to identify model parameters. Wang et al. [23] proposed an adaptive particle swarm optimization differential evolution algorithm (ADPSODE) to better identify parameters for LIBs. Using a first-order RC ECM, the relationship between open circuit voltage (OCV) and time during dynamic testing is calculated, and an optimization objective function is established to minimize the error between real and optimized terminal voltages. Xia et al. [24] proposed an improved parameter identification method to improve the accuracy of the model. Using nonlinear least squares method to determine model parameters based on pulse discharge experimental data. Zhang et al. [25] extracted some key parameters from the driving process of electric vehicles that are helpful for global optimization method initialization and upper and lower limit settings, and designed an improved particle swarm optimization method for periodically updating model parameters during constant charging (CC) process. Although online parameter identification methods have been widely studied, continuous current load is required for online parameter identification, which increases the complexity of testing and model uncertainty. Therefore, the most commonly used method currently is offline identification of battery parameters. In the offline parameter identification method, the battery model parameters are usually obtained by performing a pulse discharge process and conducting hybrid pulse power characteristic (HPPC) testing based on the transient response of terminal voltage. Sun et al. [26] employed the Taguchi method to study the influence of four HPPC parameters (positive and negative pulse heights, pulse length, and relaxation length) on ECM performance under various operating conditions (dynamic, non-dynamic, and quasi-static tests). Hu et al. [27] proposed a LIB parameter identification method that combines MATLAB and 1stOpt software to eliminate the impact of inaccurate initial parameter values on the parameter identification results of LIB models. This method fully utilizes the powerful global optimization ability of 1stOpt to obtain accurate initial parameter values. Wang et al. [28] utilized a combination of polynomial fitting and single-factor sensitivity analysis to quantitatively investigate the sensitivity of different model performance metrics in the ECM to three model parameters at various states of charge. However, it should be noted when using offline parameter identification methods that offline parameter identification requires calculating the parameters of the battery through pulse discharge. For example, when using a second-order ECM, it is necessary to fit the pulse length and relaxation length of the discharge pulse of HPPC. Accurate initial value setting of the fitting function is necessary to calculate the second-order equivalent circuit time constant. Therefore, accurate initial value setting is crucial for offline parameter

identification methods. In addition, accurate battery parameters play an important role in battery model construction and SOC estimation.

Currently, the ECM is commonly used in conjunction with filtering algorithms for estimating the SOC of batteries. Due to the outstanding noise-filtering properties of the Kalman filtering algorithm, many researchers have applied it to battery SOC estimation. However, traditional Kalman filtering algorithms (KF) can only address linear system problems, while batteries exhibit non-linear characteristics, and the SOC of batteries is influenced by these non-linear characteristics. Therefore, in order to expand the applicability of KF to nonlinear systems, extended Kalman filtering (EKF) algorithm and unscented Kalman filtering (UKF) algorithm nonlinear system algorithms were introduced for SOC estimation. Shi et al. [29] proposed an adaptive extended Kalman filter (AEKF) based SOC estimation method for LIBs to address issues such as the selection of forgetting factors, robustness, and susceptibility to noise in the EKF algorithm. By introducing the noise adaptive algorithm into the EKF algorithm, the SOC is estimated based on the recognition results and applied in the next parameter recognition, iteratively executing to achieve accurate estimation of SOC. E et al. [30] estimated SOC based on the EKF algorithm for OCV. Then, a Simscape battery model was established to estimate battery parameters, and the accuracy of SOC estimation was verified through HPPC experiments. The simulation results show that under active equalization, the dispersion of SOC in the discharge stage decreases from 7.4% to 4.12%, and the maximum error of this SOC estimation method is about 4%. However, due to the linearization process in the EKF algorithm, it introduced linearization errors, which can lead to algorithm divergence. But the UKF algorithm addresses the issues related to linearization by utilizing the Unscented Transform (UT) to compute covariance and mean values, avoiding linearization errors, and effectively improving SOC estimation accuracy. Peng et al. [31] developed an adaptive unscented Kalman filter (AUKF) based on noise statistical estimator and model parameter regulator to accurately estimate the SOC of series battery systems. When the previous noise statistics of AUKF are inaccurate or not entirely Gaussian, use a noise statistical estimator to adaptively obtain its estimated noise statistics. By comparing the developed AUKF and UKF, the accuracy and effectiveness of the SOC estimation method were verified. When the system statistical noise is random, AUKF can accurately track the reference SOC.

Wang et al. [32] proposed an adaptive robust unscented Kalman filter (ARUKF) based on multi parameter updates. The weight function of the institute of geodesy and geophysics (IGGIII) is introduced as a robust factor into the UKF to adjust the weight of observation residuals, and an adaptive filter tuning based on the backward horizon is used to obtain time-varying noise covariance. When the initial error of SOC is 20 %, the convergence speed of SOC estimation using ARUKF is faster than that using UKF. Although UKF improves the accuracy of SOC estimation compared to EKF, but there is an inaccurate problem with the mean and covariance results obtained by UKF after the sigma points approximate probability distribution transformation, which can affect the accuracy and stability of SOC estimation using UKF.

Through a review of existing literature, there is a lack of research on the impact of differences in the initial value setting of offline parameter identification fitting functions on the estimation of battery voltage in second-order ECMs. Inaccurate initial value setting of functions directly affects the solution results of parameter identification functions, resulting in inaccurate estimation of voltage. Additionally, due to the instability of the UKF algorithm in its UT process and the influence of process noise and observation noise on the UKF algorithm, there are issues related to low accuracy and instability in using UKF for battery SOC estimation. In order to solve the above problems and achieve accurate battery SOC prediction, this paper focuses on a simple and accurate method for determining the initial value of offline parameter identification fitting functions. In addition, based on the obtained parameter identification results, a LIB second-order ECM and a modified UKF simulation model were established. The innovation and primary

**Table 1**  
Battery parameters.

Type specification	NCM	LFP
Rated capacity (Ah)	26.5	5
Rated voltage (V)	3.7	3.3
Maximum current (A)	132.5	25
Charging cut-off voltage (V)	4.2	3.7
Discharge cut-off voltage (V)	2.7	2.7

**Table 2**  
HPPC test profile for the NCM battery.

Step no.	Step name	Duration	Current	Cut-off condition
1	Constant current discharge	/	1/2 C	$V \leq 2.7$ V
2	Rest	30 min	/	/
3	Constant current charge	/	1/2 C	Current $\leq 1.0$ A
4	Rest	30 min	/	/
5	Constant current discharge	10 s	3 C	/
6	Rest	40 s	/	/
7	Constant current discharge	12 min	1/2 C	/
8	Rest	30 min	/	/
9	Constant current discharge	10 s	3 C	/
10	Rest	40 s	/	/
11	Constant current charge	10 s	2 C	/
12	Rest	40 s	/	/
13	Repeat steps 7–12 for 9 times			
14	Constant current discharge	/	1/2 C	$V \leq 2.7$ V
15	Rest	30 min	/	/
16	Constant current charge	10 s	2 C	/
17	Rest	40 s	/	/
18	Constant current discharge	/	1/2 C	$V \leq 2.7$ V
19	Rest	30 min	/	/

**Table 3**  
HPPC test profile for the LFP battery.

Step no.	Step name	Duration	Current	Cut-off condition
1	Constant current discharge	/	1/2 C	$V \leq 2.7$ V
2	Rest	60 min	/	/
3	Constant current charge	/	1/2 C	Current $\leq 1.0$ A
4	Rest	60 min	/	/
5	Constant current discharge	10 s	3 C	/
6	Rest	40 s	/	/
7	Constant current discharge	6 min	1 C	/
8	Rest	30 min	/	/
9	Constant current discharge	10 s	3 C	/
10	Rest	40 s	/	/
11	Constant current charge	10 s	3 C	/
12	Rest	40 s	/	/
13	Repeat steps 7–12 for 9 times			
14	Constant current discharge	/	1 C	$V \leq 2.7$ V
15	Rest	60 min	/	/
16	Constant current charge	10 s	3 C	/
17	Rest	40 s	/	/
18	Constant current discharge	/	1 C	$V \leq 2.7$ V
19	Rest	60 min	/	/

contributions of this study are as follows:

(1) A pseudo random initial value combined with least squares fit LIB parameter identification method is proposed in order to eliminate the influence of uncertainty in initial parameter values on the parameter identification results in the HPPC curve of LIB.

(2) The UKF model modified by a first order low pass filtering (FOLPF) algorithm is introduced to improve the accuracy and stability of battery SOC estimation.

(3) The proposed method has good applicability for SOC estimation of both NCM and LFP batteries.

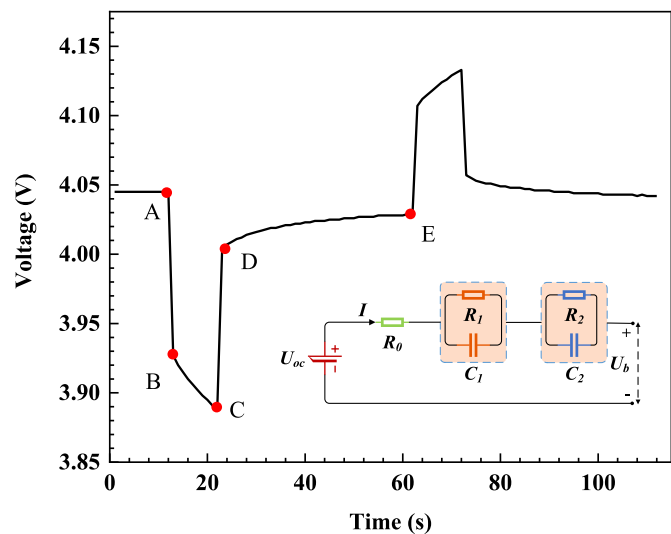


**Fig. 1.** Voltage response diagram of pulse discharge.

The remaining sections of this paper are organized as follows: Section 2 presents the details of the experimental design. Then, in Section 3, the second-order ECM, UKF, and the principle of first-order low-pass filtering algorithm were introduced. The results are presented and analyzed in Section 4. Section 5 concludes this paper and lists some directions for future research.

## 2. Experiments

### 2.1. Experimental subjects

Two different types of LIBs were used in HPPC experiments in this paper. The first battery is a LFP soft pack battery, and the other battery is an aluminum shell NCM battery. The specific battery parameters are shown in Table 1.

### 2.2. HPPC discharge experiment

The HPPC experimental testing equipment is managed by the Bitrode Cell Tester (MCV 2–200–5, USA). The BMS is responsible for collecting voltage, current data, and time information of the battery, and transmitting the information to the terminal computer through a data converter (Netgear JFS524, USA). The data sampling frequency is set to 1 second, and both batteries are tested at an ambient temperature of 25 °C. Firstly, a 1/3 C capacity calibration test is performed on the NCM battery. Before the discharge HPPC test is conducted, the battery capacity is fully discharged at a rate of 1/2 C. After a break of 30 minutes, the battery is fully charged at a 1/2 C rate. Finally, the battery undergoes a pulse test at every 0.1 SOC interval until the capacity is depleted. Two different HPPC testing conditions are used, namely full pulse and single pulse. The full pulse HPPC testing steps for NCM battery are shown in Table 2, while the single pulse misses steps 11 and 12 compared to the full pulse.

Similarly, before conducting HPPC testing on LFP batteries, a 1/3 C capacity calibration test is performed. Then the battery capacity is fully discharged at a rate of 1/2 C. After a break of 60 minutes, a charging rate of 1/2 C is used to complete battery charging. To avoid the impact of the LFP battery voltage platform on the terminal voltage, the break time for full charge and the break time for discharge end are set to 60 minutes respectively. Finally, a pulse test is conducted for every 0.1 SOC reduction in battery capacity until the capacity is depleted. The HPPC test steps for full pulse discharge of LFP batteries are shown in Table 3, while the single pulse misses steps 11 and 12 compared to the full pulse.

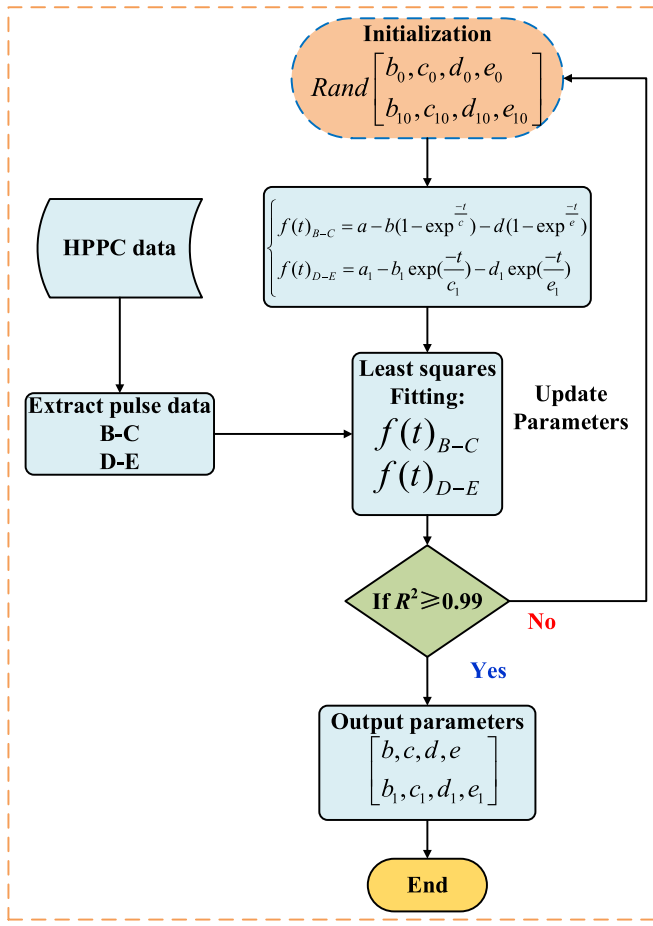


Fig. 2. Parameter identification process.

### 3. Modeling algorithms

#### 3.1. Parameter identification

The accurate estimation of SOC largely depends on the accuracy and complexity of the ECM. Although the commonly used Thevenin and PNGV models can simulate the electrochemical reactions inside the battery, their effectiveness is not satisfactory. In addition, the third-order ECM is too complex and not conducive to the establishment of the model. Compared with the second-order ECM, the accuracy of the third-order model did not significantly improve [33]. Therefore, considering the trade-off between accuracy and complexity of the model, the second-order RC model in the ECM is chose in this paper, which can accurately simulate the polarization effect of the battery. The algorithm is relatively simple and easy to implement in engineering. The second-order ECM is shown in Fig. 1. The  $U_{oc}$  is OCV,  $U_b$  is terminal voltage,  $I$  is current,  $R_0$  is internal resistance,  $R_1$  and  $R_2$  are polarization resistors, and  $C_1$  and  $C_2$  are polarization capacitors. Eqs. (1), (2) and (3) can be obtained through Kirchhoff's law.

$$U_{oc} = IR_0 + U_1 + U_2 + U_b \quad (1)$$

$$I = \frac{U_1}{R_1} + C_1 \frac{dU_1}{dt} \quad (2)$$

$$I = \frac{U_2}{R_2} + C_2 \frac{dU_2}{dt} \quad (3)$$

Where  $U_1$ , and  $U_2$  are the voltages generated by,  $R_1$ ,  $C_1$ , and  $R_2$ ,  $C_2$ , respectively,  $U_b$  is terminal voltage.

When pulse discharge is experienced by LIB, the change in battery

Table 4

Main steps of UKF implementation.

Step no.	
Step 1	Initialize the mean $\bar{x}$ and covariance $P$ of the state variables: $\hat{\bar{x}}_0 = E[\bar{x}_0]$ $P_0 = E[(\bar{x}_0 - \hat{\bar{x}}_0)(\bar{x}_0 - \hat{\bar{x}}_0)^T]$
Step 2	2 n+1 Sigma sampling points obtained by UT transform: $\begin{cases} X_{i,k-1} = \hat{\bar{x}}_{k-1}, i = 0 \\ X_{i,k-1} = \hat{\bar{x}}_{k-1} + (\sqrt{n + \lambda(P_{X,k-1})})_i, i = 1, 2, \dots, n \\ X_{i,k-1} = \hat{\bar{x}}_{k-1} - (\sqrt{n + \lambda(P_{X,k-1})})_i, i = n+1, n+2, \dots, 2n \end{cases}$
Step 3	Further prediction of state quantities and covariance matrix: $\begin{cases} \hat{\bar{x}}_{k/(k-1)} = f(X_{k-1,i}, u_{k-1}) \\ \hat{\bar{X}}_{k/(k-1)} = \sum_{i=0}^{2n} \omega_{m,i} X_{k/(k-1),i} \\ P_{k/(k-1)} = \sum_{i=0}^{2n} \left[ \omega_{c,i} [\hat{\bar{x}}_{k/(k-1)} - X_{k/(k-1),i}] \right] \left[ [\hat{\bar{x}}_{k/(k-1)} - X_{k/(k-1),i}]^T + Q_k \right] \end{cases}$
Step 4	Compute the mean value of the system prediction: $\begin{cases} Y_{k/(k-1),i} = g(X_{k-1,i}, u_{k-1}) \\ Y_{k/(k-1)} = \sum_{i=0}^{2n} \omega_{m,i} Y_{k/(k-1),i} \end{cases}$
Step 5	Compute the mutual covariance matrix and covariance matrix: $\begin{cases} P_{ykyk} = \sum_{i=0}^{2n} \left[ \omega_{c,i} [\hat{\bar{Y}}_{k/(k-1),i} - Y_{k/(k-1)}] \right] \left[ [\hat{\bar{Y}}_{k/(k-1),i} - Y_{k/(k-1)}]^T + R_k \right] \\ P_{xkyk} = \sum_{i=0}^{2n} \left[ \omega_{c,i} [X_{k/(k-1),i} - \hat{\bar{X}}_{k/(k-1)}] \right] \left[ [X_{k/(k-1),i} - \hat{\bar{X}}_{k/(k-1)}]^T \right] \end{cases}$
Step 6	Compute the Kalman gain matrix $K$ : $K_k = P_{xkyk} P_{ykyk}^{-1}$
Step 7	Update the state matrix and error covariance matrix: $\begin{cases} \hat{\bar{x}}_k = Y_{k/(k-1)} + K_k (Y_k - Y_{k/(k-1)}) \\ P_{k+1} = P_{k/(k-1)} - K_k P_{ykyk} K_k^T \end{cases}$

terminal voltage is shown in Fig. 1. Due to the presence of ohmic internal resistance, the  $R_0$  terminal voltage suddenly drops from A to B. Similarly, at the end of the discharge, due to the presence of  $R_0$ , the terminal voltage suddenly rises from C to D. Therefore,  $R_0$  can be calculated by Ohm's law as shown in Eq. (4).

$$R_0 = \frac{(U_A - U_B) + (U_D - U_C)}{2I} \quad (4)$$

Where  $U_A$ ,  $U_B$ ,  $U_C$ , and  $U_D$  represent the terminal voltages at points A, B, C, and D, respectively, and  $I$  represent the current during pulse discharge.

There are two special stages in the pulse discharge process, corresponding to the two stages B-C and D-E in Fig. 1. The main reason for these two special stages is the existence of polarization internal resistance inside the battery, which leads to a hysteresis effect in the voltage. Two RC circuits are used in the ECM to simulate the polarization internal resistance of the battery. The B-C stage is a process where the battery voltage slowly decreases at the beginning of discharge, and there is still current flowing through the circuit during this stage. The voltage description equation for the zero state response in the corresponding RC circuit is shown in Eqs. (5), (6) and (7).

$$\tau_1 = R_1 C_1 \quad (5)$$

$$\tau_2 = R_2 C_2 \quad (6)$$

$$U_b = U_{oc} - IR_0 - IR_1 \left( 1 - \exp^{-\frac{t}{\tau_1}} \right) - IR_2 \left( 1 - \exp^{-\frac{t}{\tau_2}} \right) \quad (7)$$

Where  $\tau_1$  and  $\tau_2$  are the time constant of two RC circuits.

The D-E stage is the process of slowly increasing the battery voltage

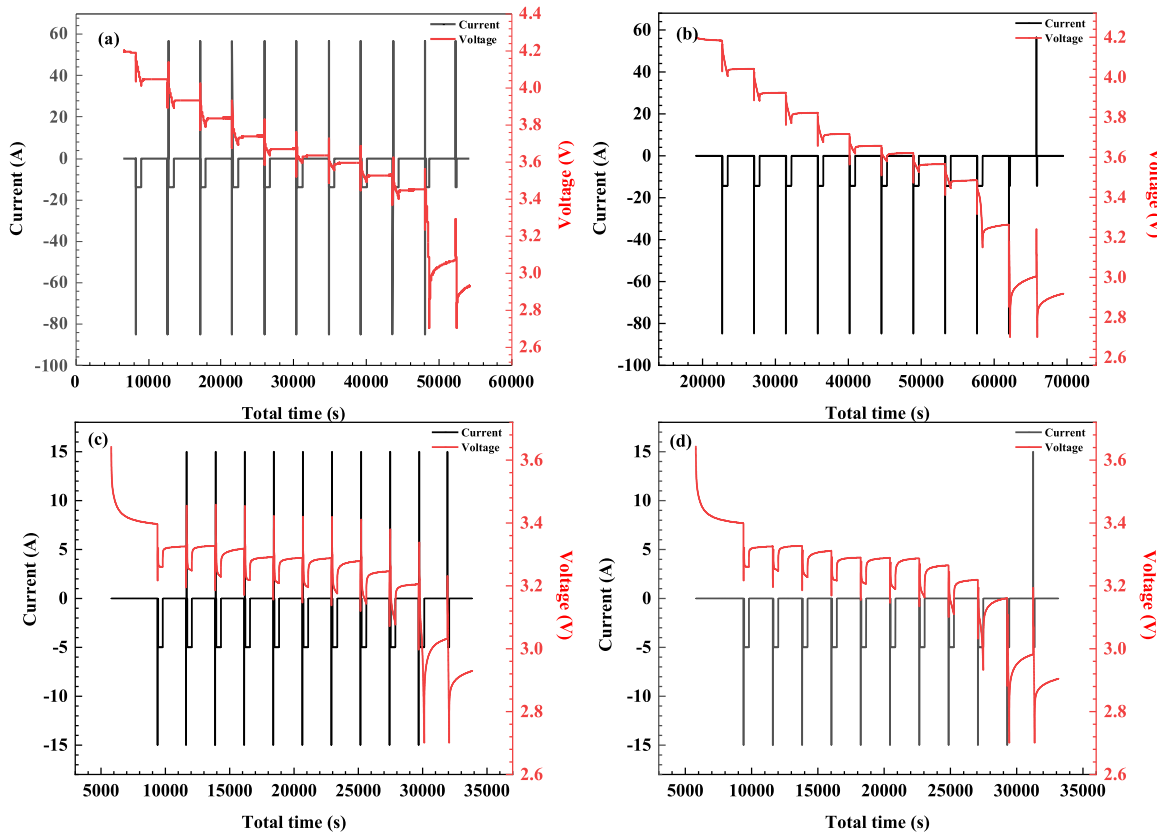


**Fig. 3.** Two types of HPPC test results for NCM battery and LFP batteries. (a) is the full pulse test curve of the NCM battery; (b) is the single pulse test curve of NCM battery; (c) is the full pulse test curve of the LFP battery; (d) is the single pulse test curve of LFP battery.

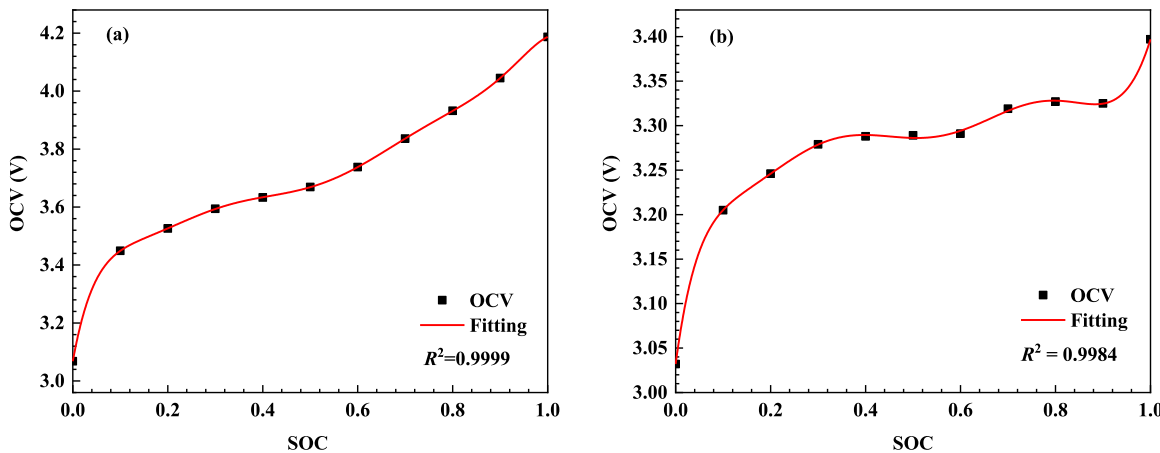


**Fig. 4.** OCV-SOC fitting results of NCM and LFP batteries. (a) NCM battery OCV-SOC fitting results; (b) LFP battery OCV-SOC fitting results.

at the end of discharge, during which no current flows through the circuit. The voltage description equation for the zero input response in the corresponding RC circuit is shown in Eq. (8).

$$U_b = U_{oc} - U_1 \exp\left(\frac{-t}{\tau_1}\right) - U_2 \exp\left(\frac{-t}{\tau_2}\right) \quad (8)$$

Where  $U_1$  and  $U_2$  are the voltages generated by  $R_1 C_1$  and  $R_2 C_2$ , respectively.

By analyzing the ECM, the voltage description equations for the zero state response stage (B-C) and zero input response stage (D-E) can be obtained. By fitting and solving the voltage description functions for the B-C and D-E stages, the model parameters in the RC circuit of the

equivalent circuit can be identified. The solution function constructed based on the B-C and D-E stages is shown in Eq. (9).

$$\begin{cases} f(t)_{B-C} = a - b(1 - \exp^{\frac{-t}{c}}) - d(1 - \exp^{\frac{-t}{e}}) \\ f(t)_{D-E} = a_1 - b_1 \exp\left(\frac{-t}{c_1}\right) - d_1 \exp\left(\frac{-t}{e_1}\right) \end{cases} \quad (9)$$

Where  $a = U_{oc} - IR_0$ ,  $a_1 = U_{oc}$ ,  $b = IR_1$ ,  $b_1 = U_1$ ,  $d = IR_2$ ,  $d_1 = U_2$ ,  $c = \tau_{1(B-C)}$ ,  $e = \tau_{2(B-C)}$ ,  $c_1 = \tau_{1(D-E)}$ ,  $e_1 = \tau_{2(D-E)}$ .

The value of  $U_{oc}$  can be calculated through the fitting polynomial of OCV and SOC, and the identification of other parameters in the equation can be obtained by solving Eq. (9). Equations  $f(t)_{B-C}$  and  $f(t)_{D-E}$  are solved through curve fitting using the least squares method using T-V

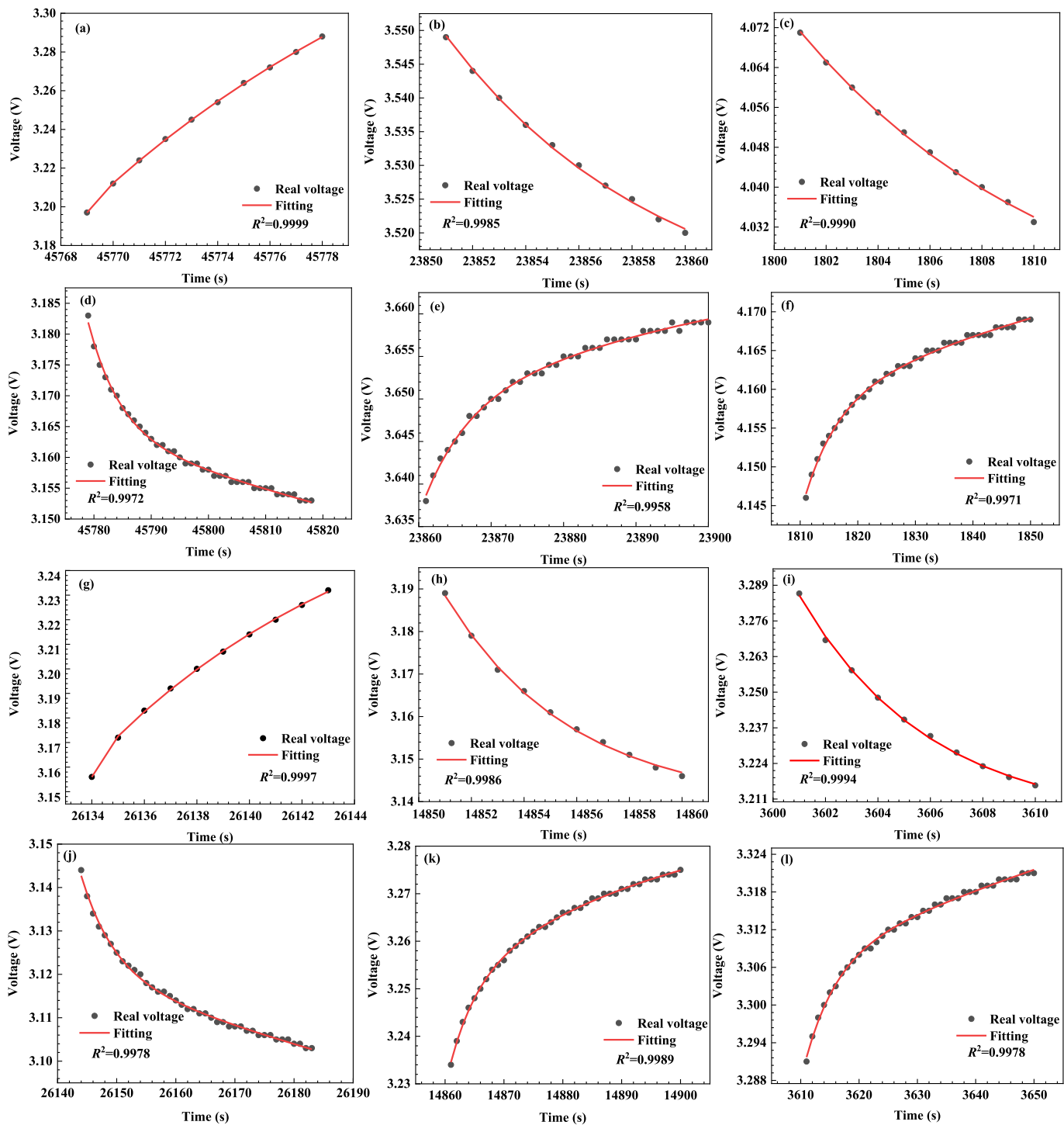


**Fig. 5.** Pulse fitting results of NCM and LFP batteries under different SOC. (a, d) and (g, j) are the pulse fitting result of NCM and LFP batteries at 0.0 SOC; (b, e) and (h, k) are the pulse fitting result of NCM and LFP batteries at 0.5 SOC; (c, f) and (i, l) are the pulse fitting result of NCM and LFP batteries at 1.0 SOC.

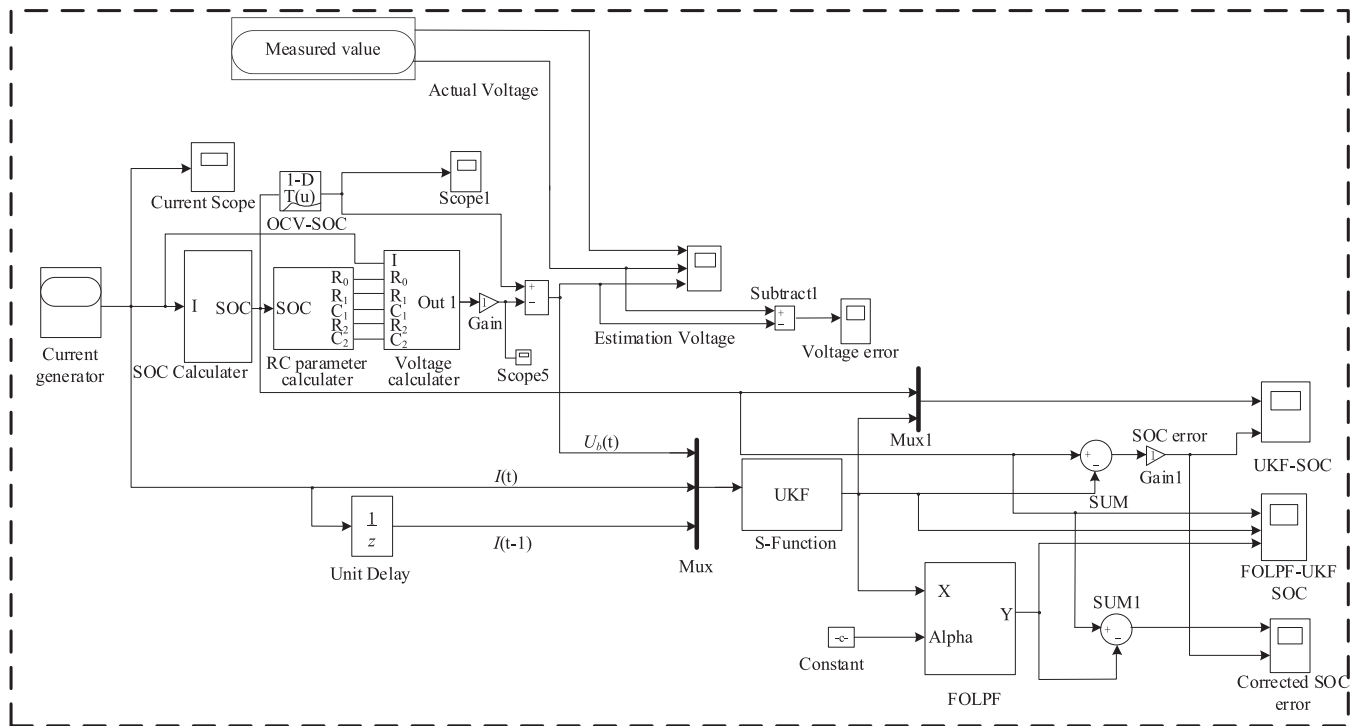
**Table 5**  
NCM battery parameter identification results.

SOC	0.0	0.1	0.2	0.3	0.4	0.5	0.6	0.7	0.8	0.9	1.0
$R_0$	0.001378	0.001796	0.001496	0.001425	0.001402	0.001402	0.001413	0.001402	0.001396	0.001372	0.001349
$b$	0.2226	0.01598	0.005923	0.004163	0.05594	0.004823	0.06318	0.1057	0.07080	0.06433	0.08144
$d$	0.2360	0.1376	0.0603	0.06142	0.003818	0.04829	0.004571	0.003119	0.006192	0.006278	0.004705
$c_1$	328.5288	4.8213	99.7474	5.5438	6.1491	53.8651	6.4838	62.4137	6.9345	71.7343	5.7315
$e_1$	5.6894	66.4568	8.6397	66.5227	57.8560	6.0652	91.8235	5.4021	71.2496	5.6945	82.5273

**Table 6**

LFP battery parameter identification results.

SOC	0.0	0.1	0.2	0.3	0.4	0.5	0.6	0.7	0.8	0.9	1.0
$R_0$	0.0071	0.0081	0.0073	0.0068	0.0065	0.0063	0.0060	0.0062	0.0059	0.0057	0.0062
$b$	0.2242	0.1219	0.08517	0.07177	0.06631	0.06081	0.05628	0.06848	0.06635	0.05759	0.03298
$d$	0.1375	0.01913	0.01029	0.007377	0.005738	0.004486	0.005273	0.004037	0.006198	0.005619	0.08224
$c_1$	5.5908	3.1320	3.9845	46.4971	44.6165	4.6263	4.4837	55.3679	4.3913	29.3685	5.3984
$e_1$	177.0571	43.5216	49.6424	4.8407	4.7886	40.0213	36.2578	4.9840	33.3249	4.4546	231.9526

**Fig. 6.** Simulation model for estimating SOC using second-order ECM.

data from the pulse discharge process, in order to make the initial values of curve equations  $f(t)_{B-C}$  and  $f(t)_{D-E}$  simpler and more accurate, the RAND function in MATLAB is used to set the pseudo random initial value of Eq. (9). The Rand function randomly generates pseudo random numbers that follow a uniform distribution between 0 and 1. The pseudo random array is used as the initial value for solving the curve equation, and then the fitting is calculated using the least squares method. The optimal fit of Eq. (9) to B-C and D-E voltage data is the accurate identification result. The Pearson correlation coefficient ( $R^2$ ) is used as the basis for optimal fitting. The closer the absolute value of  $R^2$  is to 1, the more accurate the identification result is. Therefore, the cutoff condition is to cycle off when the  $R^2$  is greater than 0.99. Then the parameters  $b$ ,  $d$ ,  $c_1$  and  $e_1$  in equations Eq. (9) can be easily and accurately identified, the specific implementation process is shown in Fig. 2. The values of  $R_1$ ,  $C_1$ ,  $R_2$ , and  $C_2$  can be calculated by Eq. (10).

$$\begin{cases} R_1 = \frac{b}{I} \\ R_2 = \frac{d}{I} \\ C_1 = \frac{c_1}{R_1} \\ C_2 = \frac{e_1}{R_2} \end{cases} \quad (10)$$

Where  $c_1 = \tau_{1(D-E)}$  and  $e_1 = \tau_{2(D-E)}$ .

### 3.2. A modified UKF algorithm for SOC estimation

UT is used by UKF to describe the Gaussian distribution of random variables, a set of Sigma sampling points are used, and then through the transfer of nonlinear functions, weighted statistical linear regression techniques are used to approximate the posterior mean and variance of nonlinear functions [34]. For a nonlinear system, the state equation and measurement equation for additional noise are shown in Eq. (11).

$$\begin{cases} x_k = f(x_{k-1}, u_k) + \omega_k \\ y_k = g(x_k, u_k) + \nu_k \end{cases} \quad (11)$$

Where  $f(\bullet)$  is the nonlinear system state transition equation;  $g(\bullet)$  is a nonlinear measurement equation;  $x_k$  is the state variable;  $u_k$  is a known input;  $y_k$  is the measurement signal;  $k$  is the current moment;  $\omega_k$  is Gaussian process noise with zero mean;  $\nu_k$  is a Gaussian measurement noise with zero mean.

The specific steps for estimating battery SOC using UKF are shown in the Table 4.

Although UKF has good applicability for estimating battery SOC, there are also problems such as unstable estimation results and divergent results. This is reflected in the fact that the UT process cannot fully simulate the actual data distribution, which increases the uncertainty of SOC estimation. The error between the estimated voltage calculated by the second-order equivalent circuit and the real voltage can affect the accuracy of UKF estimation of battery SOC. In addition, the artificially introduced process noise and measurement noise in the UKF algorithm

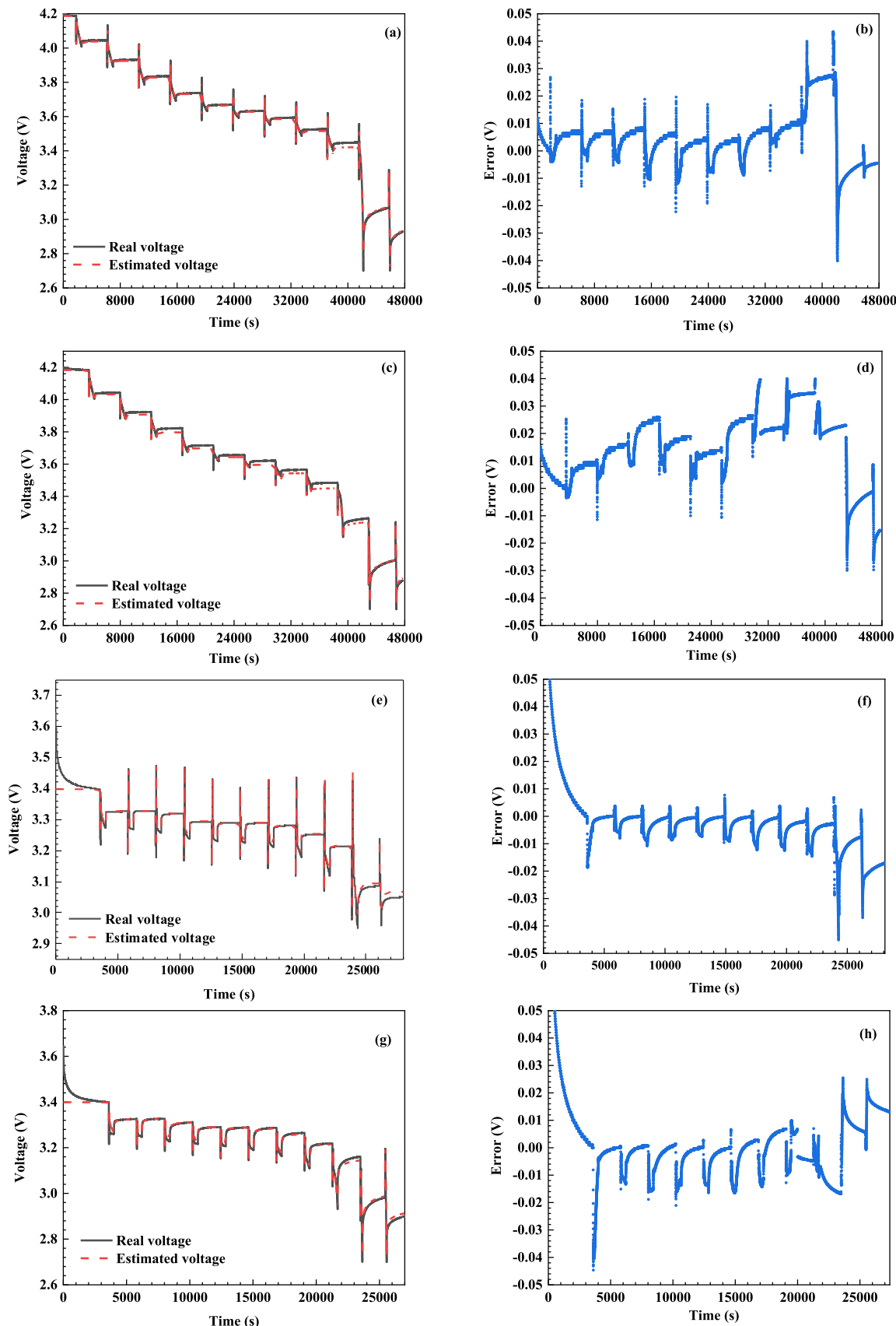


**Fig. 7.** Voltage estimation results and errors of NCM and LFP batteries. (a, b) are under full pulse testing of NCM battery; (c, d) are under single pulse testing of NCM battery; (e, f) are under full pulse testing of LFP battery; (g, h) are under single pulse testing of LFP battery.

**Table 7**

Evaluation criteria for voltage estimation of NCM and LFP batteries.

Battery type	HPPC test	RMSE / V	MAE / V
NCM	full pulse	0.009943	0.007334
	single pulse	0.01889	0.01648
LFP	full pulse	0.007877	0.005107
	single pulse	0.01695	0.008811

can also affect the estimation results of battery SOC. In particular, smaller simulation steps are generally used in order to obtain more accurate simulation results. Due to the existence of the above errors, the UKF algorithm cannot achieve accurate SOC estimation.

The FOLPF algorithm corrects outliers in SOC estimation results and reduces noise by weighting the current estimation results and previous filtering results. The FOLPF algorithm uses a filtering coefficient  $\alpha$  to achieve the mathematical expression of result correction, as shown in Eq. (12).

$$SOC_{(t)} = \alpha UKF[SOC_{(t)}] + (1 - \alpha)SOC_{(t-1)} \quad (12)$$

Where  $SOC_{(t)}$  is the current correction value,  $UKF[SOC_{(t)}]$  is the current estimated value,  $\alpha$  is the correction coefficient, and  $SOC_{(t-1)}$  is the previous correction value.

### 3.3. The evaluation criteria of estimation

Error, mean absolute error (MAE) and root mean square error (RMSE) are used to evaluate the voltage and SOC estimation performance of the parameters identification and corrected UKF model [35]. The calculation formulas of error, MAE and RMSE are as Eqs. (13), (14) and (15).

$$Error = Estimated_i - Real_i \quad (13)$$

$$MAE = \frac{\sum_{i=1}^n |Estimated_i - Real_i|}{n} \quad (14)$$

$$RMSE = \sqrt{\frac{1}{n} \sum_{i=1}^n (Estimated_i - Real_i)^2} \quad (15)$$

Where  $i$  represents the current estimated voltage or estimated SOC sequence number,  $Estimated_i$  represents the estimated voltage or SOC value,  $Real_i$  represents the real voltage or SOC value, and  $n$  represents the total number of estimated voltage or estimated SOC.

## 4. Results and discussion

The results of two types of HPPC tests conducted by NCM and LFP batteries at 25 °C are shown in Fig. 3. Compared with double pulse HPPC tests, single pulse HPPC tests have fewer positive pulse processes, resulting in fewer steps for single pulse tests than double pulse tests. The experimental testing process is simple, and the time cost is lower than that of double pulse tests. In order to fully identify the parameters of LIB, positive and negative pulses were added for NCM and LFP batteries when SOC was equal to 1.0 and SOC was equal to 0.0. Identifies the parameters of NCM and LFP batteries offline through full pulse testing conditions, and then verifies the accuracy of model parameter identification by loading single pulse current conditions in this paper.

Based on HPPC testing to obtain data on OCV and SOC, there will be a corresponding rest process after each 0.1 SOC discharge, in order to restore the voltage to a stable state through rest, and the stabilized voltage is approximately equal to OCV. The OCV-SOC curves of NCM and LFP batteries during discharge at an ambient temperature of 25 °C are shown in Fig. 4. The relationship between SOC and OCV is fitted using an eighth order polynomial. The fitting results of NCM and LFP batteries are shown in Eqs. (16) and (17).

$$\begin{aligned} \text{NCM: } & \text{OCV} = -418.8858 \times \text{SOC}^8 + 1784.1448 \times \text{SOC}^7 - \\ & 3132.0100 \times \text{SOC}^6 + 2926.9154 \times \text{SOC}^5 - 1572.7933 \times \text{SOC}^4 + 429.9649 \times \text{SOC}^3 - \\ & 88.2287 \times \text{SOC}^2 + 9.0117 \times \text{SOC} + 3.0680 \end{aligned} \quad (16)$$

$$\begin{aligned} \text{LFP: } & \text{OCV} = -130.0125 \times \text{SOC}^8 + 611.9035 \times \text{SOC}^7 - \\ & 1164.5253 \times \text{SOC}^6 + 1159.0704 \times \text{SOC}^5 - 651.5220 \times \text{SOC}^4 + 209.4527 \times \text{SOC}^3 - \\ & 37.9828 \times \text{SOC}^2 + 3.9810 \times \text{SOC} + 3.0320 \end{aligned} \quad (17)$$

Based on HPPC test data, pseudo random initial values were combined with the least squares method to fit and solve equations  $f(t)_{B-C}$  and  $f(t)_{D-E}$ . Fig. 5 shows the fitting results of equations in the 0.0 SOC, 0.5 SOC, and 1.0 SOC segments using the offline parameter identification method based on the initial values of pseudo random numbers proposed in this paper. It can be obtained that the fitting correlation coefficients of NCM and LFP batteries under different SOC are all above 0.99, and the correlation coefficient calculation is shown in Eq. (18).

$$R^2 = \frac{\sum_{i=1}^N (X_i - \bar{X})(Y_i - \bar{Y})}{\sqrt{\sum_i^N (X_i - \bar{X})^2} \sqrt{\sum_{i=1}^N (Y_i - \bar{Y})^2}} \quad (18)$$

where  $R^2$  is the value of the Pearson correlation coefficient between -1 and 1;  $N$  represents for the number of voltage;  $X_i$  and  $\bar{X}$  stand for real voltage and their average value;  $Y_i$  and  $\bar{Y}$  imply the estimated voltage and their average value. The greater the  $R^2$  value, the higher the correlation between the estimated voltage and real voltage.

The identification results of NCM and LFP batteries parameters are shown in Tables 5 and 6, with SOC ranging from 0.0 to 1.0. The results of  $R_1$ ,  $R_2$ ,  $C_1$ ,  $C_2$  in the second-order ECM can be calculated by identifying  $b$ ,  $d$ ,  $c_1$ ,  $e_1$  combined with Eq. 10.

After identifying all the parameters of the second-order ECM, a Simulink second-order equivalent circuit simulation model was established to estimate the voltage of NCM and LFP batteries in this paper. At the same time, the modified UKF algorithm is combined with the simulation model to estimate the battery SOC. In order to visualize the correction of UKF by the FOLPF algorithm, a FOLPF model is constructed to achieve the correction of UKF estimation results, and the simulation model is shown in Fig. 6.

The voltage estimation results and errors of the simulation model are shown in Fig. 7, with a simulation step size of 0.04. The voltage estimation results of NCM battery under full pulse and single pulse HPPC tests are shown in Fig. 7(a, c), while the voltage estimation results of LFP battery under full pulse and single pulse HPPC tests are shown in Fig. 7(e, g). The estimated voltage curve has a good matching effect with the real voltage curve, and the identified parameters of NCM and LFP batteries can effectively describe the voltage changes. From the error curve, it can be seen that the maximum error of NCM battery voltage estimation does not exceed 0.04 V. In addition, the maximum error of LFP battery voltage estimation does not exceed 0.045 V.

The performance of voltage estimation for NCM batteries and LFP batteries under two types of HPPC testing are shown in Table 7. The RMSE result of the estimated voltage for NCM batteries is below 0.0190 V, and the MAE value is below 0.0170 V. The RMSE of the estimated voltage is less than 0.0170 V for LFP batteries while the MAE value is less than 0.0090 V.

The SOC estimation results of NCM and LFP batteries based on UKF and modified UKF are shown in Fig. 8. The range of  $\alpha$  is between 0 and 1. The smaller the filtering coefficient, the more stable the filtering result is. The larger the filtering coefficient, the more sensitive the result is. To ensure stability and sensitivity, the value of the  $\alpha$  was set to 0.002 and the simulation step size was set to 0.04 through simulation testing. The SOC estimation error increases if the step size is greater than 0.04. However, the SOC estimation efficiency decreases when the step size is less than 0.04. Therefore, the step size is set to 0.04 after the estimation error of SOC and computational efficiency is weighed. The SOC

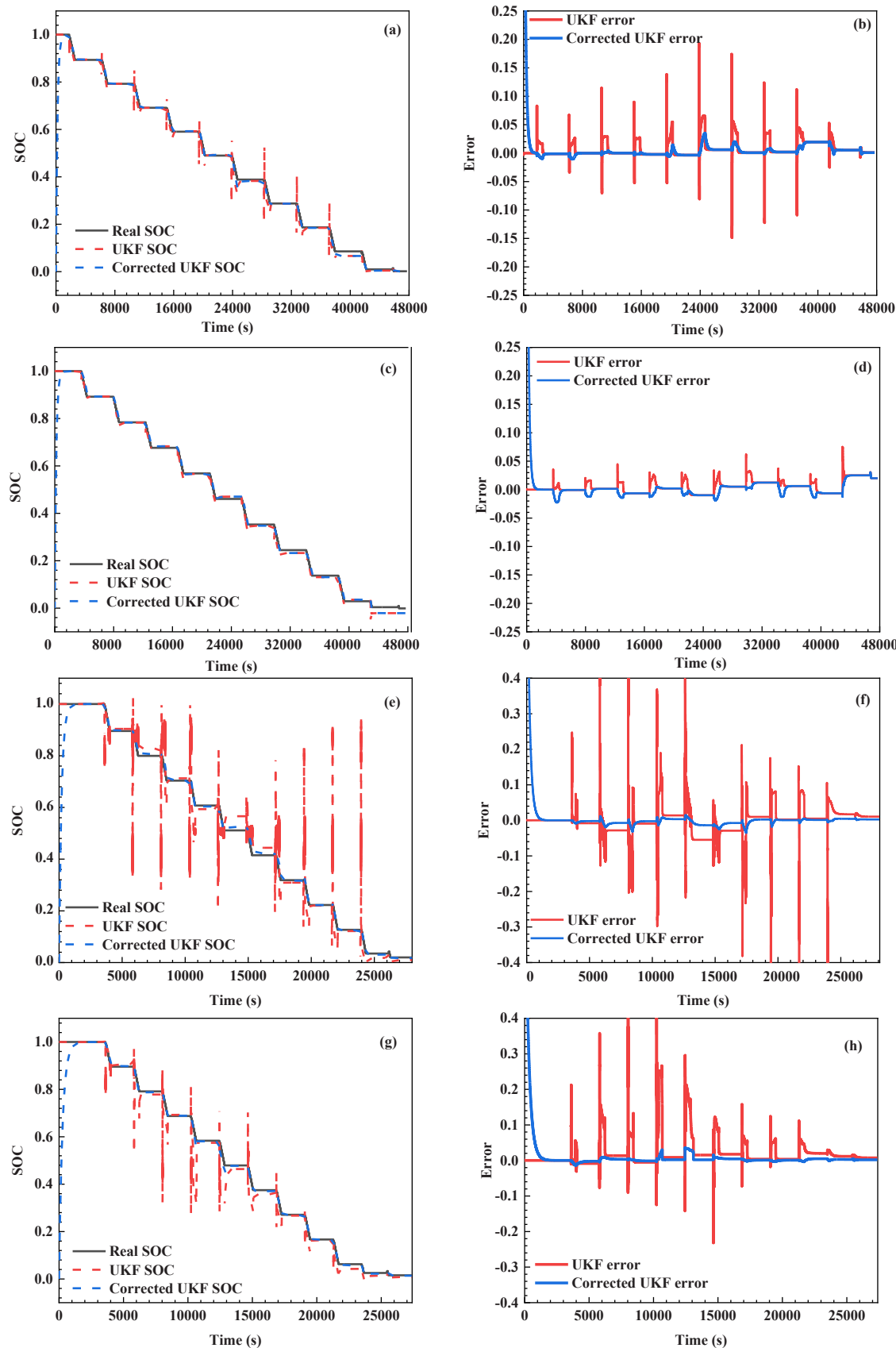


**Fig. 8.** SOC estimation results and errors of NCM and LFP batteries. (a, b) are under full pulse testing of NCM battery; (c, d) are under single pulse testing of NCM battery; (e, f) are under full pulse testing of LFP battery; (g, h) are under single pulse testing of LFP battery.

**Table 8**

Evaluation criteria for SOC estimation based on corrected UKF for NCM and LFP batteries.

Battery type	HPPC test	RMSE	MAE
NCM	full pulse	0.008037	0.004957
	single pulse	0.009485	0.007443
LFP	full pulse	0.007708	0.005554
	single pulse	0.006547	0.003769

**Table 9**

Comparative review of the modified UKF with other existing SOC estimation methods.

Method	Battery type	RMSE	MAE	Reference
LSTM&UKF	LFP	0.0094	0.0082	[17]
AEKF	LCO	0.0341	0.0105	[29]
RUKF	NCM	0.0223	0.0183	[32]
IAUKF	NCM	0.0113	0.0097	[35]
FOLPF&UKF	NCM	0.0095	0.0074	This work
	LFP	0.0077	0.0055	

estimation results of NCM battery based on UKF and modified UKF are shown in Fig. 8(a, c), and the SOC estimation results of LFP battery based on UKF and modified UKF are shown in Fig. 8(e, g). The error curve of SOC estimation between NCM and LFP batteries are shown in Fig. 8(b, d, f, h), it can be seen that due to the instability of UKF and the unavoidable estimation voltage error, there is a significant fluctuation in the SOC estimation results of UKF, which increases the estimation error of SOC. The fluctuations and outliers in the SOC estimation results based on the modified UKF have been corrected, effectively improving the estimation accuracy of SOC. The maximum error of SOC estimation for both NCM and LFP batteries is within 0.025, and the stability of SOC estimation results has also been improved, which can be seen from the error graphs.

The RMSE and MAE results of NCM and LFP batteries based on modified UKF estimation of battery SOC are shown in Table 8. The SOC estimation results of NCM batteries based on modified UKF under two test conditions have a maximum RMSE value of 0.0094 and a maximum MAE value of 0.0074. The SOC estimation results of LFP battery based on modified UKF under two test conditions have a maximum RMSE value of 0.0077 and a maximum MAE value of 0.0055.

The comparison of the evaluation accuracy of different methods for SOC estimation in the literature are shown in Table 9. In the above references, SOC estimation results for different types of batteries were obtained through different methods. It can be seen from Table 9 that the error of the method proposed in this paper is relatively low.

## 5. Conclusions

The UKF model modified by a FOLPF algorithm is introduced to improve the accuracy and stability of battery SOC estimation. The applicability and robustness of the proposed method are explored in HPPC data of different battery types. The conclusions are drawn as follow.

(1) The pseudo random number generated by the RAND function is used as the initial value of the parameter identification equation, and the parameter identification of LIBs is achieved through least squares fitting. It is found that the goodness of fit between the true and estimated HPPC pulse voltage values at different SOC values for both NCM and LFP batteries is above 0.99.

(2) Based on the parameter identification results, the maximum absolute error of the HPPC voltage estimated by the second-order ECM is within 0.045 V under both full pulse and single pulse testing conditions.

(3) The UKF model modified by the FOLPF algorithm can effectively improve the accuracy of SOC estimation for NCM and LFP batteries, with a maximum absolute error of SOC estimation within 0.025.

(4) Environmental temperature and battery SOH are also important

factors affecting the accurate estimation of battery SOC. This work only explores the precise SOC estimation of new NCM and LFP batteries using the proposed UKF model modified by the FOLPF algorithm at room temperature. The SOC estimation of this algorithm under different temperature and battery SOH will be discussed to verify its applicability in future work.

## Declaration of Competing Interest

Authors have no conflict of interest to declare (i) No support, financial or otherwise, has been received from any organization that may have an interest in the submitted work; (ii) There are no other relationships or activities that could appear to have influenced the submitted work.

## Acknowledgements

This work was sponsored by the Science and Technology Commission of Shanghai Municipality (19DZ2271100), the Science and Technology Support Program of Guizhou Province ([2022] General 15, [2022] General 12) and Shanghai Key Laboratory of Materials Protection and Advanced Materials in Electric Power, China.

## References

- [1] Y. Xiao, J. Wen, L. Yao, J. Zheng, Z. Fang, Y. Shen, A comprehensive review of the lithium-ion battery state-of-health prognosis methods combining aging mechanism analysis, *J. Energy Storage* 65 (2022) 107347 <https://doi.org/10.1016/j.est.2023.107347>.
- [2] S. Yang, C. Zhang, J. Jiang, W. Zhang, L. Zhang, Y. Wang, Review on state-of-health of lithium-ion batteries: characterizations, estimations and applications, *J. Clean. Prod.* 314 (2021) 128015 <https://doi.org/10.1016/j.jclepro.2021.128015>.
- [3] C. Wang, S. Wang, J. Zhou, J. Qiao, X. Yang, Y. Xie, A novel back propagation neural network-dual extended Kalman filter method for state-of-charge and state-of-health co-estimation of lithium-ion batteries based on limited memory least square algorithm, *J. Energy Storage* 59 (2023) 106563 <https://doi.org/10.1016/j.est.2022.106563>.
- [4] X. Li, L. Ju, G. Geng, Q. Jiang, Data-driven state-of-health estimation for lithium-ion battery based on aging features, *Energy* 274 (2023) 127378 <https://doi.org/10.1016/j.energy.2023.127378>.
- [5] J. Tian, R. Xiong, W. Shen, J. Lu, X.G. Yang, Deep neural network battery charging curve prediction using 30 points collected in 10 min, *Joule* 5 (2021) 1521–1534, <https://doi.org/10.1016/j.joule.2021.05.012>.
- [6] Y. Xie, S. Wang, G. Zhang, Y. Fan, C. Fernandez, J.M. Guerrero, Improved lumped electrical characteristic modeling and adaptive forgetting factor recursive least squares-linearized particle swarm optimization full-parameter identification strategy for lithium-ion batteries considering the hysteresis component effect, *J. Energy Storage* 67 (2023) 107597 <https://doi.org/10.1016/j.est.2023.107597>.
- [7] T. Ouyang, P. Xu, J. Chen, J. Lu, N. Chen, Improved parameters identification and state of charge estimation for lithium-ion battery with real-time optimal forgetting factor, *Electrochim. Acta* 353 (2020) 136576 <https://doi.org/10.1016/j.electacta.2020.136576>.
- [8] R. Xiong, Y. Duan, K. Zhang, D. Lin, J. Tian, C. Chen, State-of-charge estimation for onboard LiFePO<sub>4</sub> batteries with adaptive state update in specific open-circuit-voltage ranges, *Appl. Energy* 349 (2023) 121581 <https://doi.org/10.1016/j.apenergy.2023.121581>.
- [9] X. Pang, X. Liu, J. Jia, J. Wen, Y. Shi, J. Zeng, Z. Zhao, A lithium-ion battery remaining useful life prediction method based on the incremental capacity analysis and Gaussian process regression, *Microelectron. Reliab.* 127 (2021) 114405 <https://doi.org/10.1016/j.microrel.2021.114405>.
- [10] C. Hu, Y. Xing, D. Du, X. Si, J. Zhang, Remaining useful life estimation for two-phase nonlinear degradation processes, *Reliab. Eng. Syst. Saf.* 230 (2023) 108945 <https://doi.org/10.1016/j.ress.2022.108945>.
- [11] W. Dang, S. Liao, B. Yang, Z. Yin, M. Liu, L. Yin, W. Zheng, An encoder-decoder fusion battery life prediction method based on Gaussian process regression and improvement, *J. Energy Storage* 59 (2023) 106469 <https://doi.org/10.1016/j.est.2022.106469>.
- [12] P. Takyi-Aninakwa, S. Wang, H. Zhang, H. Li, X. Yang, C. Fernandez, An ASTSEKF optimizer with nonlinear condition adaptability for accurate SOC estimation of lithium-ion batteries, *J. Energy Storage* 70 (2023) 108098 <https://doi.org/10.1016/j.est.2023.108098>.
- [13] M.S. Hossain Lipu, S. Ansari, M.S. Miah, S.T. Meraj, K. Hasan, A.S.M. Shihavuddin, M.A. Hannan, K.M. Muttaqi, A. Hussain, Deep learning enabled state of charge, state of health and remaining useful life estimation for smart battery management system: Methods, implementations, issues and prospects, *J. Energy Storage* 55 (2022) 105752 <https://doi.org/10.1016/j.est.2022.105752>.

- [14] C. Wang, N. Cui, Z. Cui, H. Yuan, C. Zhang, Fusion estimation of lithium-ion battery state of charge and state of health considering the effect of temperature, *J. Energy Storage* 53 (2022) 105075 <https://doi.org/10.1016/j.est.2022.105075>.
- [15] P. Takyi-Aninakwa, S. Wang, G. Liu, A.N. Bage, F. Masahudu, J.M. Guerrero An, enhanced lithium-ion battery state-of-charge estimation method using long short-term memory with an adaptive state update filter incorporating battery parameters, *Eng. Appl. Artif. Intell.* 132 (2024) 107946 <https://doi.org/10.1016/j.engappai.2024.107946>.
- [16] Z. Cui, L. Kang, L. Li, L. Wang, K. Wang, A combined state-of-charge estimation method for lithium-ion battery using an improved GRU network and UKF, *Energy* 259 (2022) 124933 <https://doi.org/10.1016/j.energy.2022.124933>.
- [17] F. Yang, S. Zhang, W. Li, Q. Miao, State-of-charge estimation of lithium-ion batteries using LSTM and UKF, *Energy* 201 (2020) 117664 <https://doi.org/10.1016/j.energy.2020.117664>.
- [18] Y. Li, K. Li, X. Liu, X. Li, L. Zhang, B. Rente, T. Sun, K.T.V. Grattan, A hybrid machine learning framework for joint SOC and SOH estimation of lithium-ion batteries assisted with fiber sensor measurements, *Appl. Energy* 325 (2022) 119787 <https://doi.org/10.1016/j.apenergy.2022.119787>.
- [19] X. Liu, K. Li, J. Wu, Y. He, X. Liu, An extended Kalman filter based data-driven method for state of charge estimation of Li-ion batteries, *J. Energy Storage* 40 (2021) 102655 <https://doi.org/10.1016/j.est.2021.102655>.
- [20] D.V.S.R. Sesidhar, B. Chandrashekhar, C.Robert Green II, A review on data-driven SOC estimation with Li-Ion batteries: implementation methods & future aspirations, *J. Energy Storage* 72 (2023) 108420 <http://doi.org/10.1016/j.est.2023.108420>.
- [21] X. Lai, J. Weng, Y. Huang, M. Yuan, Y. Yao, X. Han, Y. Zheng, A joint state-of-health and state-of-energy estimation method for lithium-ion batteries through combining the forgetting factor recursive least squares and unscented Kalman filter, *Measurement* 205 (2022) 112187 <https://doi.org/10.1016/j.measurement.2022.112187>.
- [22] J. Shi, H. Guo, D. Chen, Parameter identification method for lithium-ion batteries based on recursive least square with sliding window difference forgetting factor, *J. Energy Storage* 44 (2021) 103485 <https://doi.org/10.1016/j.est.2021.103485>.
- [23] C. Wang, M. Xu, Q. Zhang, J. Feng, R. Jiang, Y. Wei, Y. Liu, Parameters identification of Thevenin model for lithium-ion batteries using self-adaptive particle swarm optimization differential evolution algorithm to estimate state of charge, *J. Energy Storage* 44 (2021) 103244 <https://doi.org/10.1016/j.est.2021.103244>.
- [24] B. Xia, C. Chen, Y. Tian, M. Wang, W. Sun, Z. Xu, State of charge estimation of lithium-ion batteries based on an improved parameter identification method, *Energy* 90 (2015) 1426–1434, <https://doi.org/10.1016/j.energy.2015.06.095>.
- [25] S. Zhang, Q. Zhang, D. Liu, X. Dai, X. Zhang, State-of-charge estimation for lithium-ion battery during constant current charging process based on model parameters updated periodically, *Energy* 257 (2022) 124770 <https://doi.org/10.1016/j.energy.2022.124770>.
- [26] J. Sun, J. Kainz, Optimization of hybrid pulse power characterization profile for equivalent circuit model parameter identification of Li-ion battery based on Taguchi method, *J. Energy Storage* 70 (2023) 108034 <https://doi.org/10.1016/j.est.2023.108034>.
- [27] Z. Hu, G. Ren, J. Zhang, Y. Si, Y. Duan, A parameter identification and state of charge estimation method of lithium-ion battery considering temperature bias, *J. Energy Storage* 68 (2023) 107650 <https://doi.org/10.1016/j.est.2023.107650>.
- [28] J. Wang, Y. Jia, N. Yang, Y. Lu, M. Shi, X. Ren, D. Lu, Precise equivalent circuit model for Li-ion battery by experimental improvement and parameter optimization, *J. Energy Storage* 52 (2022) 104980 <https://doi.org/10.1016/j.est.2022.104980>.
- [29] N. Shi, Z. Chen, M. Niu, Z. He, Y. Wang, J. Cui, State-of-charge estimation for the lithium-ion battery based on adaptive extended Kalman filter using improved parameter identification, *J. Energy Storage* 45 (2022) 103518 <https://doi.org/10.1016/j.est.2021.103518>.
- [30] J.E., B. Zhang, Y. Zeng, M. Wen, K. Wei, Z. Huang, J. Chen, H. Zhu, Y. Deng, Effects analysis on active equalization control of lithium-ion batteries based on intelligent estimation of the state-of-charge, *Energy* 238 (2022) 121822 <https://doi.org/10.1016/j.energy.2021.121822>.
- [31] S. Peng, X. Zhu, Y. Xing, H. Shi, X. Cai, M. Pecht, An adaptive state of charge estimation approach for lithium-ion series-connected battery system, *J. Power Sources* 392 (2018) 48–59, <https://doi.org/10.1016/j.jpowsour.2018.04.101>.
- [32] L. Wang, J. Ma, X. Zhao, X. Li, K. Zhang, Z. Jiao, Adaptive robust unscented Kalman filter-based state-of-charge estimation for lithium-ion batteries with multi-parameter updating, *Electrochim. Acta* 426 (2022) 140760 <https://doi.org/10.1016/j.electacta.2022.140760>.
- [33] V. Selvaraj, I. Vairavasundaram, A comprehensive review of state of charge estimation in lithium-ion batteries used in electric vehicles, *J. Energy Storage* 72 (2023) 108777 <https://doi.org/10.1016/j.est.2023.108777>.
- [34] M. Hossain, M.E. Haque, M.T. Arif, Kalman filtering techniques for the online model parameters and state of charge estimation of the Li-ion batteries: A comparative analysis, *J. Energy Storage* 51 (2022) 104174 <https://doi.org/10.1016/j.est.2022.104174>.
- [35] J. Li, M. Ye, X. Ma, Q. Wang, Y. Wang, SOC estimation and fault diagnosis framework of battery based on multi-model fusion modeling, *J. Energy Storage* 65 (2023) 107296 <https://doi.org/10.1016/j.est.2023.107296>.